PRESSURE SCREEN-STREAMVANE INTERACTION EFFECTS ON DOWNSTREAM FLOW DISTORTION PATTERN

Elizabeth K. Mack, John Gillespie, Dustin J. Frohnapfel, Walter O'Brien, Alexandrina Untaroiu

Abstract

In order to better simulate combined pressure and swirl inlet distortions in turbofan engines, a Computational Fluid Dynamics (CFD) study was conducted to observe the effects of streamwise separation distance between a total pressure distortion screen and a StreamVane™ swirl distortion generator. A build up approach was utilized in the computational methodology. First, and isolated pressure distortion was modeled and compared to the experimental data; this served as validation for modeling the pressure screen as a porous domain. Next, an isolated StreamVane was modeled to serve as a baseline swirl distortion. Finally, a case study was conducted on the combined pressure screen ScreenVane™ configuration to determine the effects of streamwise separation distance on the generation and development of distortions downstream of the devices. The results of this study are intended to offer design guidance for future ScreenVane devise by determining the most suitable separation distance.

Nomenclature

ρ	=	density of material [kg/m^3]
$\boldsymbol{U}$	=	Velocity vector for fluid [m/s]
λ	=	Thermal conductivity [W/(m·K)]
μ	=	dynamic viscosity [kg/(m·s)]
p_∞	=	freestream pressure [Pa]
S_M	=	External momentum source [kg·m/s]
S_E	=	External energy source [kg·m^2/s^2]
δ	=	Identity Matrix or Kronecker Delta function
τ	=	Stress Tensor [N/m^2]

Introduction

Due to the need for increased fuel efficiency, boundary layer ingesting (BLI) aircraft have been a subject of much research in recent years. By ingesting some of the low-velocity boundary layer flow, the overall aircraft drag is reduced, potentially leading to increased net propulsive efficiency [1-3]. However, operating in this reduced energy flow environment poses significant challenges. The flow entering the engine is no longer uniform, but contains elements of both pressure and swirl distortion [4]. These distortions have adverse effects on the turbofan engine: reducing performance, efficiency, and design margins, as well as increasing dynamic stresses on the fan. As a result, it is critical to accurately quantify the response of a turbofan engine to the distortion profiles that it will experience when in flight [5-7].

Ground testing an engine with a complete inlet at true flight conditions is an expensive and time-consuming task. As inlet characteristics become increasingly complex, tests of this nature may become impossible without great confidence in the engine and engine inlet mechanics. A variety of devices intended to produce inlet conditions matching those encountered by the full airframe in flight have been created to fill the requirement of accurately testing an engine in a relatively simple ground test [8,9]. Two such devices are wire mesh screens and StreamVanes. Wire mesh screens (also referred to as pressure screens) are created by layering wire mesh sections on top of a backer screen. These areas of varying mesh create a tailored pressure distortion. StreamVanes consist of a tailored pattern of turning vanes designed to induce the appropriate swirl distortion profile.

As realistic inlet installations produce both swirl and pressure distortions, it has become desirable to replicate both flow conditions simultaneously during ground testing. This is achieved by installing a pressure screen upstream of a StreamVane, creating a new device known as a ScreenVane. Due to possible nonlinear interactions between the wire mesh screen and the turning vanes, a CFD study was conducted to observe the effects of streamwise separation distance on the generation and development of the combined distortions. For the CFD study, the same StreamVane and screen were analyzed at a variety of separation distances, and the resulting swirl and pressure distortion profiles were evaluated. These results may be used to make recommendations on what the separation distance should be when utilizing ScreenVanes. The following sections detail the CFD methodology, validation, and resulting flow conditions exiting a ScreenVane with varying streamwise separation distances. Finally, conclusions are presented to offer design guidance for future ScreenVane devices.

Methodology

To characterize the interaction between the pressure screen and the StreamVane, the study was broken into three sections. First, an isolated pressure distortion screen was modeled and compared to the experimental data; this served as a validation of the porous media CFD pressure screen domain. Next, an isolated StreamVane was modeled to serve as a baseline swirl distortion. Finally, a case study was conducted on the combined pressure screen StreamVane (ScreenVane) to determine the effects of streamwise separation distance on the generation and development of distortions downstream of the devices.

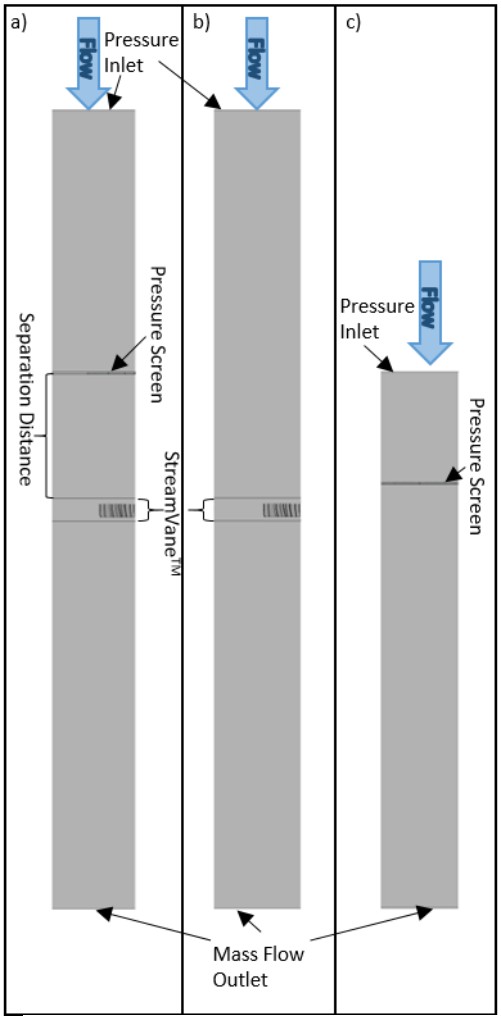

Fig. 1 a) Pressure Screen, b) StreamVane, and c) ScreenVane Models

CFD Set up

The models for this study were constructed in ANSYS CFX using CAD generated pressure screen and StreamVane geometries. Examples of the CFD models for each of the three cases can be seen in Fig. 1. The models were set up such that the upstream and downstream flow could be modeled without obstruction. For the isolated pressure screen model, the upstream duct length, of 1.43 diameters, was set to match that found in the study conducted by Bailey [10]. The downstream length was modeled to be slightly shorter than the duct length used by Bailey, at 5.5 diameters instead of 9 diameters, yet long enough to ensure flow conditions two diameters downstream did not exhibit interference from the exit boundary condition. The isolated StreamVane model was created with a five duct diameter inlet and exit duct. These lengths were chosen to capture any potential flow blockages caused by the StreamVane as well as enable the smooth transition from modeling only the StreamVane, to modeling the ScreenVane combination. The ScreenVane combination model also had a 5 diameter duct length upstream and downstream of the StreamVane, but with the addition of the pressure screen upstream of the StreamVane.

The majority of each model was constructed using a structured mesh. However, due to its more complex geometry, the StreamVane was modeled with an unstructured mesh. The governing equations for this solution come from the conservation of mass (Equation 1), momentum (Equations 2-3), and energy (Equation 4).

$$\frac{\partial \rho}{\partial t} + \nabla \cdot (\rho \, \boldsymbol{U}) = 0 \tag{1}$$

Where ρ is density and $\boldsymbol{U}$ is the velocity vector.

$$\frac{\partial (\rho \, \boldsymbol{U})}{\partial t} + \nabla \cdot (\rho \, \boldsymbol{U} \otimes \boldsymbol{U}) = -\nabla \mathrm{p} + \nabla \cdot \tau + \boldsymbol{S_M} \tag{2}$$

Where p is the pressure, $\boldsymbol{S_M}$ is momentum from an outside source, and τ is the stress tensor given by Equation 3.

$$\tau = \mu(\nabla \boldsymbol{U} + (\nabla \boldsymbol{U})^T - \frac{2}{3}\delta \, \nabla \cdot \boldsymbol{U}) \tag{3}$$

Where μ is the dynamic viscosity and δ is the identity matrix.

$$\frac{\partial (\rho \, h_{tot})}{\partial t} - \frac{\partial \rho}{\partial t} + \nabla \cdot (\rho \, \boldsymbol{U} \, h_{tot}) = \nabla \cdot (\lambda \nabla \mathrm{T}) + \nabla \cdot (\boldsymbol{U} \cdot \tau) + \boldsymbol{U} \cdot \boldsymbol{S_M} + \boldsymbol{S_E} \tag{4}$$

Where h_{tot} is the specific total enthalpy, λ is the thermal conductivity, T is the static temperature, and S_E is the contribution of an outside energy source. ANSYS used these equations along with the material properties and states seen in Table 2 to simulate the experimental

conditions. In order to solve these equations, ANSYS uses an iterative solver to achieve a specified RMS value. After acquiring an initial result for both the pressure screen case and the StreamVane case, a grid independence study was conducted on the meshes for both cases to optimize computational efficiency and accuracy using these completed runs to initialize the solver. The reason to conduct this kind of study is twofold. First, ensuring that the results obtained are consistent between cases with different meshes decreases the likelihood of artifacts manifesting in the data and verifies the precision of the simulation. Second, because a case with a higher element count (or a finer mesh) will take more computational power and time, finding a mesh size that optimizes accurate results with shorter run time allows for a more efficient case study analysis.

When conducting the grid independence study, it was assumed that differences of less than 3% in the solutions between the cases of varying mesh densities indicated consistent results. From the grid independence study the final configuration for the pressure screen showed a less than 0.13% difference from the finer mesh sizes and the final selection for the StreamVane showed less than 1.9% difference. An example of this comparison for the pressure screen case can be found in Table 1. The final element counts for the three cases were as follows: Pressure Screen model ~9 mil, StreamVane model ~ 33 mil, and ScreenVane models ~ 34 mil. Initially, the convergence criterion was set to be when the momentum and continuity RMS residuals reached 10^{-5}. This held true for the isolated cases of both the pressure screen model and the StreamVane model. However, the increased complexity of the ScreenVane model made this criterion difficult to achieve. Therefore, for the ScreenVane model, convergence was monitored by analyzing the fluctuations of the axial velocity and the total pressure of the model.

Table 1: Grid Independence Validation Example for Pressure Screen

Elements	7358124	8942489	16433253
P1 TPR	9.86E-01	9.86E-01	9.86E-01
Diff (%)	0	0	
P2 TPR	9.67E-01	9.67E-01	9.67E-01
Diff (%)	0.01	0	
P3 TPR	9.67E-01	9.67E-01	9.67E-01
Diff (%)	-0.01	0.02	
P1 vel	1.14E+02	1.14E+02	1.14E+02
Diff (%)	0	0	
P2 vel	9.91E+01	9.89E+01	9.89E+01
Diff (%)	0.13	0	
P3 vel	9.90E+01	9.91E+01	9.89E+01
Diff (%)	-0.07	0.15	

The boundary conditions used in the models were set to mimic the conditions during the experiment conducted by Bailey [11] and can be seen in Table 2. The working fluid for this model was taken to be air as an ideal gas. The flow was modeled using the built-in k-ω SST turbulence model with inflation layers created such that the y+ values would be approximately 10. These settings were used to ensure the capture of the complex interactions between the pressure screen and the StreamVane. The total pressure at the duct inlet was set to be standard sea-level atm. and the air mass flow rate at the outlet was set to 55 lb/s to match the experimental conditions. Additionally, all solid boundaries within the computational domain (i.e. the duct walls and stream vanes) were set with a no-slip wall condition.

Table 2: Computational Matrix

Parameter	Value
Turbulence model	k-ω SST
y+ value	~ 10
Air mass Flow Rate at Outlet	54.47 lb/s
Total Pressure at Inlet (p_∞)	101.325 kPa
Process type	Isothermal
Fluid Material Properties (air)	
dynamic viscosity (μ)	1.831×10^{-5} kg/(m·s)
Specific heat capacity	1004.4 J/(kg·K)
Thermal conductivity (λ)	2.61×10^{-2} W/(m·K)
Density (ρ)	1.185 kg/m^3
Porous Media Material Properties (Steel)	
Specific heat capacity	4.34×10^{2} J/(kg·K)
Thermal conductivity (λ)	60.5 W/(m·K)
Density (ρ)	7854 kg/m^3
Porous Media Domain Properties	
Area Porosity	Isotropic

Pressure Screen and StreamVane geometries

The pressure screen used for this study can be seen in Fig. 2 and reflects the design used by Bailey. The StreamVane design used in this study can be seen in Fig. 3 and was chosen as a reasonable design to pair with the pressure profile created by the pressure screen. Additionally, this StreamVane design highlights any potential interaction between the two devices, as the swirl distortion coincides with the severe pressure distortion region. The pressure screen was modeled as 0.5 in thick porous domain with varying porosity and loss resistivity coefficients to correspond to the differing mesh densities from the experimental pressure screen. These values can be seen in Table 3 while the calculation

method can be found in the Appendix. A sensitivity study on the loss resistivity coefficient was conducted to calibrate the computational model to the experimental data. The profiles from 0.28, 1, 2, and 5 diameters downstream from the pressure screen were qualitatively compared to the profiles from the same locations from Bailey's thesis for the initial loss resistivity values. This was repeated for a 10%, 20%, and 40% decrease in the loss resistivity values. Taking into account the fact that the computational model did not simulate the rotational influences of the fan, the profiles were compared for basic recovery pressure shapes and intensities.

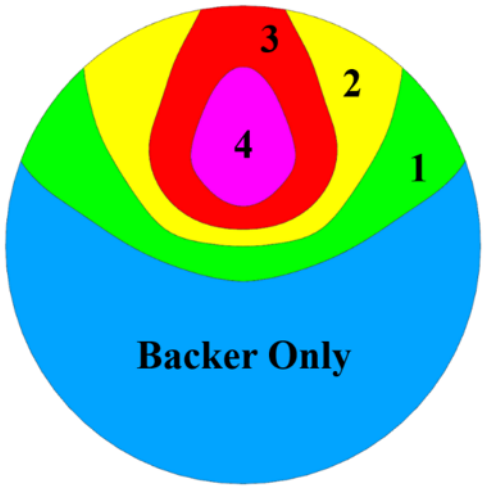

Fig. 2 Visualization of the Pressure Screen and Designations of the Different Loss Regions

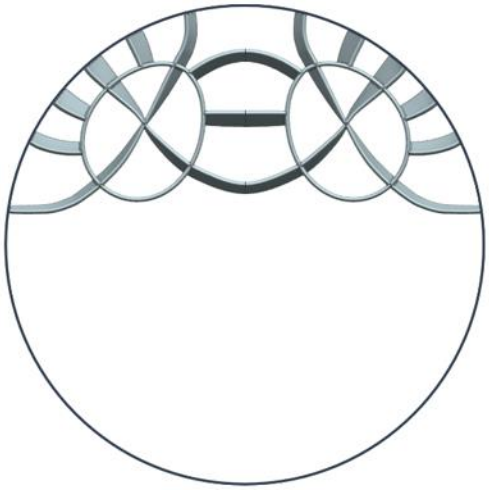

Fig. 3 Visualization of the StreamVane

For the study conducted on the streamwise separation distance for the ScreenVane, a pressure screen was added to the isolated StreamVane model at varying distances upstream. Six total streamwise separation distance cases were modeled for this study. These cases looked at the effects of the interactions within the ScreenVane when the pressure screen was located 0, 0.073, 0.273, 0.473, 0.873, and 1.673 diameters upstream of the StreamVane. These distances were chosen because the most pronounced interactions were expected to occur when the pressure screen was closer to the StreamVane.

	Resistance Loss Coefficient and Percent Reductions (m^{-1})			
Section	**Baseline**	**10%**	**20%**	**40%**
Backer	16.3	14.67	13.04	9.78
1	47.2	42.48	37.76	28.32
2	78.3	70.47	62.64	46.98
3	109.2	98.28	87.36	65.52
4	140.2	126.18	112.16	84.12

Table 3 Pressure Screen Loss Resistivity Coefficients based on Fig. 2 Designations. Porosity for Backer was 86% and porosity for sections 1-4 was 77.5%

Results and Discussion

These results show the outcomes of the sensitivity studies for the loss resistivity coefficients for the porous regions of the pressure screen as well as for the streamwise separation distances in the ScreenVane. A comparison of the profiles created with the reduced loss resistivity coefficients showed the most similar profile to the experimental results was given by the 10% reduction. A comparison of the flow distortions for the sensitivity study conducted on the ScreenVane separation distances showed a slight variation in the profiles for smaller separation distances but very little change between profiles for larger separation distance.

The pressure screen sensitivity study was conducted using estimated loss resistivity values for the 5 different sections of the pressure screen and then reducing these values by 10%, 20% and 40%. The total pressure profiles were then compared to the experimental profiles from Bailey's work[35]. The resulting profile comparison can be seen in Fig. 4. Though the profiles from the CFD do not show the blending between the different pressure sections that would be caused by the fan interactions, the pressure differentials between the simulated and experimental profiles can still be used as a basis for calibration of the loss resistivity coefficients. From Fig. 4, it can be seen that the original estimations gave too much loss compared to the experimental profiles. However, the 20% and 40% reductions did not provide enough loss. The model with a 10% reduction in the loss resistivity coefficients showed similar maximum and minimum total pressure recovery values to the experimental data, thus this model was implemented in

the creation of the ScreenVane models for the separation distance sensitivity study.

The separation distance sensitivity study results show a very slight change as the pressure screen was moved further way from the StreamVane, with the most change found between the models with smaller separation distances. Due to the nature of the two devices, there should not be much difference in radial flow angel (RFA) and the tangential flow angel (TFA) profiles downstream from the StreamVane between the model with and without the pressure screen. This can be seen in Fig. 5 and Fig. 6. Fig. 5 shows the RFA at one diameter downstream of the StreamVane trailing edge. However, a slight increase in the RFA for the area around 12 o'clock can be seen as the separation distance increases from 0 to 0.273 diameters. This increase is not as noticeable as the separation distance increases from 0.273 to 1.673. A similar trend can be seen in the TFA profiles seen in Fig. 6, a very slight change in the intensity of the angle near the origin that dissipates as the separation distance increases from 0 to 0.273 diameters and is unnoticeable as the separation distance increases from 0.273 to 1.673 diameters.

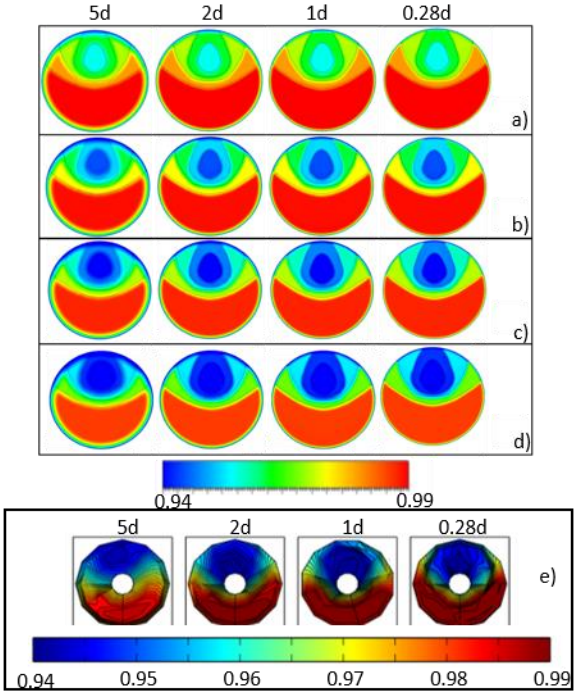

Fig. 4 Pressure Screen Sensitivity Study Profiles for the a) 40%, b) 20% c) 10%, d) 0% Loss resistivity Reduction, and e) Experimental at 5, 2, 1, and 2.8 diameters downstream of the pressure screen

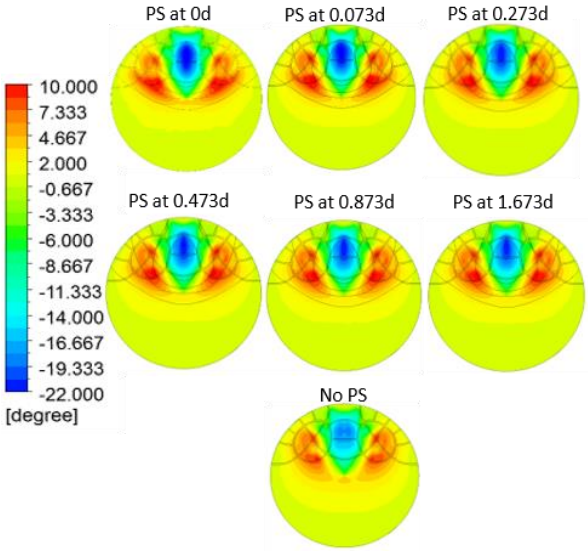

Fig. 5 Radial Flow Angle (RFA) at 1 Diameter Downstream of the StreamVane Trailing Edge

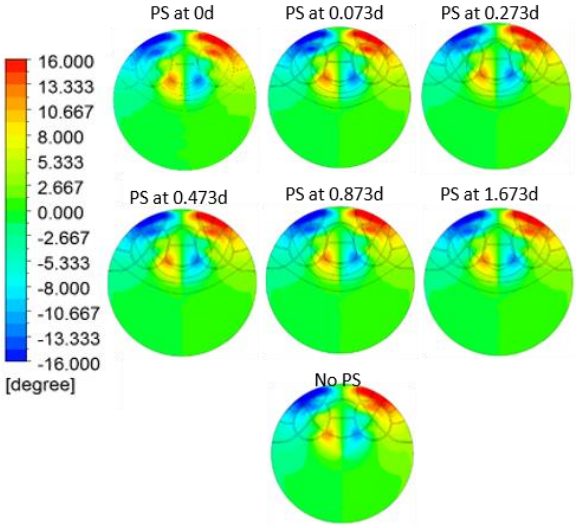

Fig. 6 Tangential Flow Angle (TFA) at 1 Diameter Downstream of the StreamVane Trailing Edge

It is expected that the pressure screen would have the most effect on the pressure recovery seen in the duct. A comparison of the pressure recovery at one diameter downstream of the StreamVane trailing edge can be seen in Fig. 7. As expected, this shows the most difference between the cases. For the case without the pressure screen, the pressure recovery is nearly 100% for the whole profile, but for the cases with the pressure screen, the influences of the pressure gradient caused by the pressure screen can be seen. Just like with the previous examples, differences can be seen between the profiles at the different separation distances. As the separation distance increases from 0 to 0.273 diameters, the inner

area of low recovery pressure increases in intensity and size. Then, as the separation distance increases from 0.473 to 0.873, the secondary low recovery pressure area is further developed and is then maintained as the separation distance increases from 0.873 to 1.673.

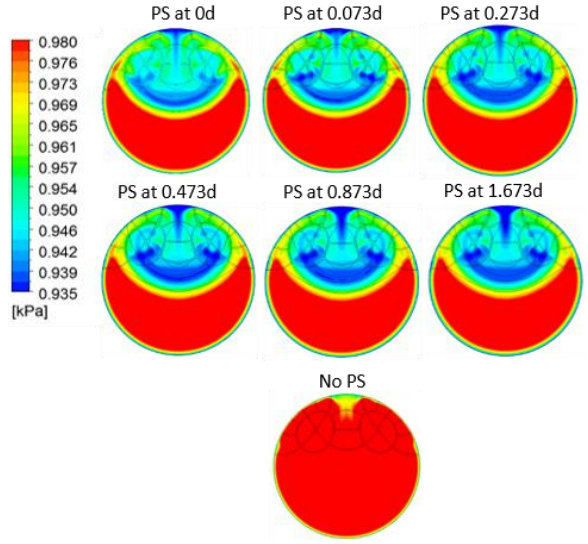

Fig. 7 Total Pressure Recovery at 1 Diameter Downstream of the StreamVane Trailing Edge

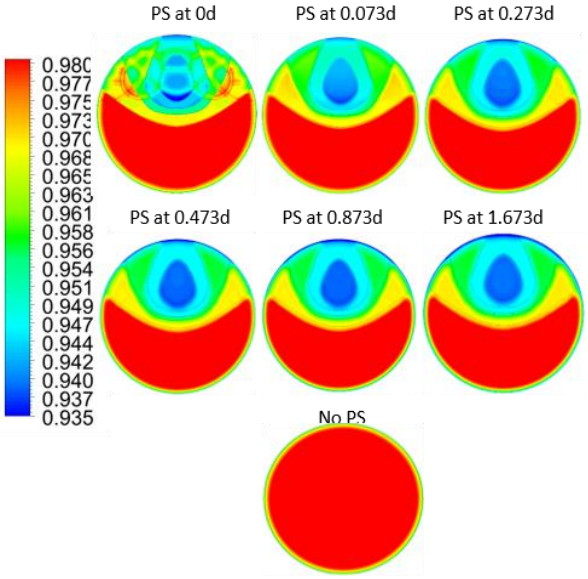

Fig. 8 Total Pressure Recovery Profiles at 0.5 in. Upstream of the StreamVane

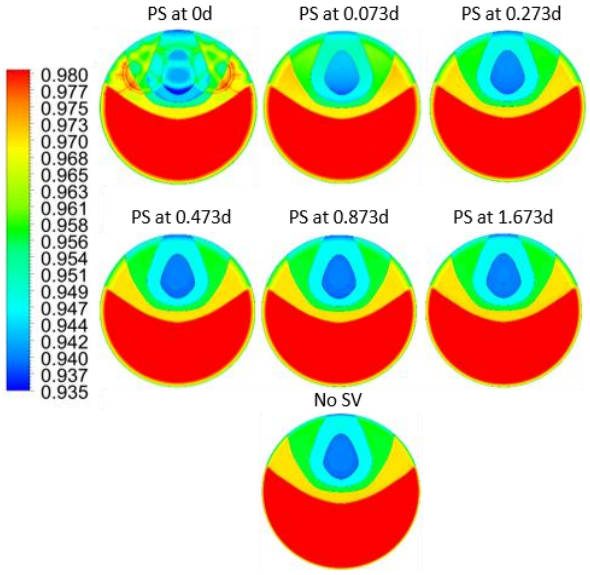

Fig. 9 Total Pressure Recovery Profiles Immediately Downstream of the Pressure Screen

This behavior can also be seen in the total pressure recovery profiles shown in Fig. 8 and Fig. 9. Fig. 8 shows larger influences from pressure screen on the area directly upstream of the StreamVane when the pressure screen was placed 0 diameters upstream of the StreamVane. From the figure, the blockage caused by StreamVane for this 0d distance is pronounced enough to see the shape of the vanes in the total pressure recovery profile. This influence greatly decreased as the pressure screen was moved to 0.073 and then 0.273 diameters upstream. When the pressure screen is located at 0.473 to 1.673 diameters upstream of the StreamVane, the profiles show little to no visible differences to the profile located at 0.273 diameters upstream. Fig. 9 shows the same story for the influences of the StreamVane on the pressure screen. The most influence from the StreamVane on the pressure profile directly behind the pressure screen can be seen when the pressure screen is located at 0 diameters upstream. Then, as the pressure screen is moved to 0.073 and 0.273 diameters upstream, this influence drastically reduces. Finally, from 0.273 to 1.673 diameters, the pressure profiles look very similar to the case without a StreamVane.

Fig. 10 shows the axial velocity profiles at the pressure screen locations for the model with only the StreamVane. Though the StreamVane, in this case, did not create as much blockage as was initially thought, there is still evidence of upstream flow distortion due to its presence. Unsurprisingly, the 0 diameter separation distance showed the most influence from the StreamVane blockage, with low to zero velocity seen directly in front of the vanes. This influence drastically decrease after the 0.073 diameter mark and becomes

almost nonexistent at 0.273 diameters upstream. The pressure screen did create an area of lower pressure immediately after its position as seen in Fig. 11. This more intense low-pressure area dissipated about 0.5 diameters downstream of the pressure screen, which coincides with the point at which the profiles became more consistent. A look at the centerline profiles as the separation distance increases also shows this kind of interaction. In Fig. 12a, the low pressure region right after the pressure screen coincides with the StreamVane region. Fig. 12b shows a significant decrease in this interaction. Fig. 12c shows the beginning of the separation of the low pressure region from the leading edge of the StreamVane. The in Fig. 12d and e, the low pressure region is completely separated from the StreamVane. It is this interaction that is the most likely cause for the differences in the profiles in Figs. 5 through 7.

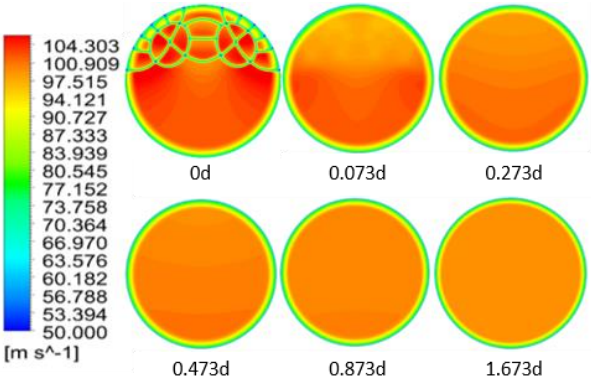

Fig. 10 Axial Velocity for Model with only the StreamVane at Upstream Pressure Screen Locations

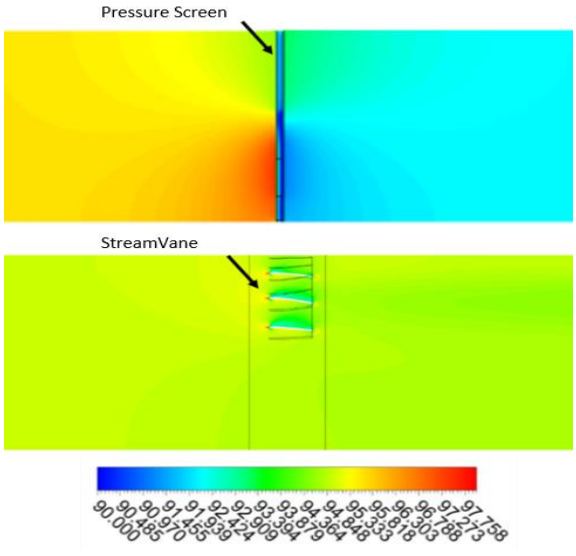

Fig. 11 Static Pressure Profiles for Pressure Screen Low Pressure Area and StreamVane Blockage (kPa)

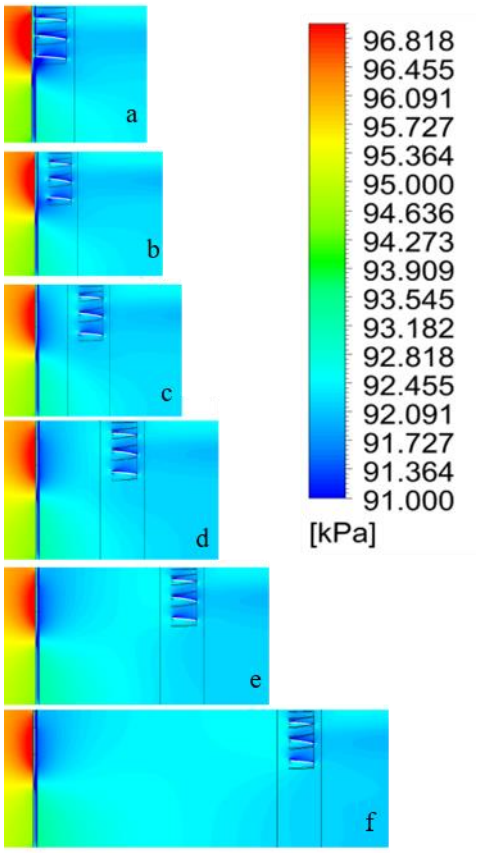

Fig. 12 Side Static Pressure Profiles of the separation area for the ScreenVane from 0 (top) to 1.673 diameters (bottom)

Conclusions

For this study, a Computational Fluid Dynamics analysis was conducted to observe the effects of streamwise separation distance on interactions between a Pressure Screen and a StreamVane and their effects on downstream flow distortions. To this end, the pressure screen and StreamVane geometries were modeled both in isolation and in combination. The isolated runs were used to obtain a baseline for the study and to validate the pressure distortion against experimental data. The ScreenVane (Pressure Screen – StreamVane combination) models focused on the influence of separation distance between the pressure screen and StreamVane on downstream flow distortions. From this study, it was proven that the presence of the Pressure Screen had minimal to no influence on the swirl distortion created by the StreamVane. This is an important observation because it means that pressure screens can be added to previously studied and generated swirl distortions without the need to re-engineer a new StreamVane. The results also showed that as the separation distance increased to over 0.473 diameters,

the presence of a lower pressure region that developed immediately after the pressure screen location ceased to influence the flow profiles downstream of the StreamVane. For this case in particular, the StreamVane itself instigated very little flow blockage, though there was still enough to see a moderate change in the axial velocity profiles as the distance from the StreamVane leading edge increased from 0 to 1.673. If a StreamVane with more vanes, for example a quad-swirl pattern, were used in this model, it is likely that the upstream flow blockage would be more pronounced. Further study of this behavior and that of the pressure screen could lead to the creation of a numerical model that predicts the influences of the blockage interaction. Through this evidence, it has shown that for ScreenVanes that utilize a StreamVane with relatively low blockage, a quarter diameter separation distance between the pressure screen and StreamVane would be sufficient to avoid the majority of the distance dependent interactions.

Appendix

The original Pressure Screen was created using steel wire mesh. The pressure screen used in the CFD analysis was estimated by modeling the pressure screen as a 0.5 in. porous plate with regions of different porosity and/or loss resistivity coefficients. The procedure for estimating the baseline loss resistivity coefficients for the pressure screen takes into account the K-value, the number of layers, the porosity of the steel wire mesh, and a porous plate of thickness 0.5 in. The porosity for each of the regions was assumed to be the smallest porosity used for that region. The initial guess for each of the regions can be seen in Table 4. The porosity for each region was assumed to be the same as the densest mesh used in the layering of the original pressure screen. The K-value for each region was calculated using the K-value for the specific wire meshes used in the pressure screen and adding them based on the number of layers of that mesh used. The 86.1% porosity (backing) mesh was found to have a K-value of 0.207 and the 77.5% porosity (layering) mesh a K-value of 0.394 from Equation 1[36].

$$K_{mesh} = \frac{1}{C^2}\left(\frac{1-\alpha^2}{\alpha^2}\right) \qquad (1)$$

Where C is a constant equal to 1.3 and α is the porosity of the mesh. The K-values for each region was then calculated using the K-values for both types of meshes in Equation 2.

$$K_{region} = K_{86.1\%} + n * K_{77.5\%} \qquad (2)$$

Where n is the number of layers of the 77.5% porosity mesh. From this, the loss resistivity coefficient (LRC) could be calculated using Equation 3.

$$LRC = K_{region}/t \qquad (3)$$

Where t is the streamwise thickness of the porous domain.

Table 4: Initial Calculations for Pressure Screen Porosity Parameters. All Layers have one layer of 86.1% porpsity

Region	Layers of 77.5% Porosity	Porosity (%)	K-value	Loss Resistivity Coefficient (m^{-1})
Backer	0	86.1	0.207	16.3
1	1	77.5	0.600	47.2
2	2	77.5	0.994	78.3
3	3	77.5	1.387	109.2
4	4	77.5	1.781	140.2

Funding Sources

This research was funded by the Virginia Space Grant Consortium from the VSGC New Investigator Program (sub-award # 18-224-100527-010) and VSGC Fellowship Award (# AT-49408). This research was also funded by Virginia Polytechnic Institute and State University through a Graduate Assistantship.

References

[1] Rodriguez, D. L., "Multidisciplinary Optimization Method for Designing Boundary-layer-Ingeting Inlets," Journal of Aircraft, Vol. 46, No. 3, 2009, pp. 883–894. doi:10.2514/1.38755

[2] Hall, C. A., Crichton, D., "Engine Design Studies for a Silent Aircraft" Journal of Tubomachinery, Vol. 129, No. 3, 2006, pp. 479–487. doi:10.1115/1.2841733

[3] Owens, L. R., Allan, B. G., and Gorton, S. A., "Boundary-Layer-Ingesting Inlet Flow Control," Journal of Aircraft, Vol. 45, No. 4, July-August 2008, pp. 1431-1440.

[4] Graitzer, E. M., Strand, T., "Asymmetric Swirling Flows in Turbomachine Annuli," Journal of Engineering for Power, Vol. 100, No. 4, 1978, pp. 618-629. doi: 10.1115/1.3446410

[5] Govardhan, M., Viswanath, K., "Investigations on an axial flow fan stage sugject to circumferenctial inlet flow distortion and swirl" Journal of Thermal Science, Vol. 6, No. 4, 1997, pp. 241–250. doi:10.1115/1.2841733

[6] Kurzke, J., "Effects of Inlet Flow Distortion on the Performance of Aircraft Gas Turbines," Journal of Engineering for Gas Turbines and Power, Vol. 130, No. 4, 2008, pp. 041201-1 - 7. doi: 10.1007/s11630-997-0003-8

[7] Hale, A., O'Brien, W., "A Three-Dimensional Turbine Engine Analysis Compressor Code (TEACC) for Steady-State Inlet Distortion," Journal of Tubomachinery, Vol. 120, No. 3, 1998, pp. 422–430. doi:10.1115/1.2841733

[8] Gunn, E. J., Tooze, S. E., Hall, C. A., and Colin, Y., "An Experimental Study of Loss Sources in a Fan Operating with Continuous Inlet Stagnation Pressure Distortion," Journal of Turbomachinery, ASME, Vol. 135, September 2013. doi: : 10.1115/1.4007835

[9] Sheoran, Y., Bouldin, B., and Krishnan, P. M., "Compressor Performance and Operability in Swirl Distortion," Journal of Turbomachinery, ASME, Vol. 134, July 2012. doi: 10.1115/1.4003657

[10] Bailey, J. M., "The Influence of Developemnt and Fan/Screen Interaction on Screen-Generated Total Pressure Distortion Profiles," Blacksburg, Virginia: Justin M. Bailey, 2013.

[11] Perry, R. H., Green, D. W., "Perry's Chemical Engineers' Handbook," Seventh Edition, McGraw-Hill Professional Publishing, June 1997. 9780070498419